

# PPGFlowECG: Latent Rectified Flow with Cross-Modal Encoding for PPG-Guided ECG Generation and Cardiovascular Disease Detection

Xiaocheng Fang<sup>1,2,\*</sup>, Jiarui Jin<sup>1,2,\*</sup>, Haoyu Wang<sup>1,4,\*</sup>, Che Liu<sup>3</sup>, Jieyi Cai<sup>1,4</sup>, Yujie Xiao<sup>1</sup>, Guangkun Nie<sup>1,2</sup>, Bo Liu<sup>2</sup>, Shun Huang<sup>1</sup>, Hongyan Li<sup>2,†</sup>, Shenda Hong<sup>1,†</sup>

<sup>1</sup>National Institute of Health Data Science, Peking University, China

<sup>2</sup>School of Intelligence Science and Technology, Peking University, China

<sup>3</sup>Data Science Institute, Imperial College London, UK

<sup>4</sup>University of Chinese Academy of Sciences, China

{hongshenda, leehy}@pku.edu.cn

## Abstract

Electrocardiography (ECG) is the clinical gold standard for cardiovascular disease (CVD) assessment, yet continuous monitoring is constrained by the need for dedicated hardware and trained personnel. Photoplethysmography (PPG) is ubiquitous in wearable devices and readily scalable, but it lacks electrophysiological specificity, limiting diagnostic reliability. While generative methods aim to translate PPG into clinically useful ECG signals, existing approaches are limited by the misalignment of physiological semantics in generative models and the complexity of modeling in high-dimensional signals. To address these limitations, we propose PPGFlowECG, a two-stage framework that aligns PPG and ECG in a shared latent space using the CardioAlign Encoder and then synthesizes ECGs with latent rectified flow. We further provide a formal analysis of this coupling, showing that the CardioAlign Encoder is necessary to guarantee stable and semantically consistent ECG synthesis under our formulation. Extensive experiments on four datasets demonstrate improved synthesis fidelity and downstream diagnostic utility. These results indicate that PPGFlowECG supports scalable, wearable-first CVD screening when standard ECG acquisition is unavailable. The code is available at <https://github.com/PKUDigitalHealth/PPGFlowECG>.

## 1 Introduction

Cardiovascular diseases (CVDs) remain the leading cause of mortality worldwide [Timmis *et al.*, 2022; Vaduganathan *et al.*, 2022; Chong *et al.*, 2024]. Continuous monitoring can enable earlier detection and timely intervention [Bayoumy *et al.*, 2021]. Although electrocardiography (ECG) is the diagnostic gold standard, routine deployment is constrained by the need for specialized equipment and trained personnel [Kligfield *et al.*, 2007]. Wearable ECG devices have improved ac-

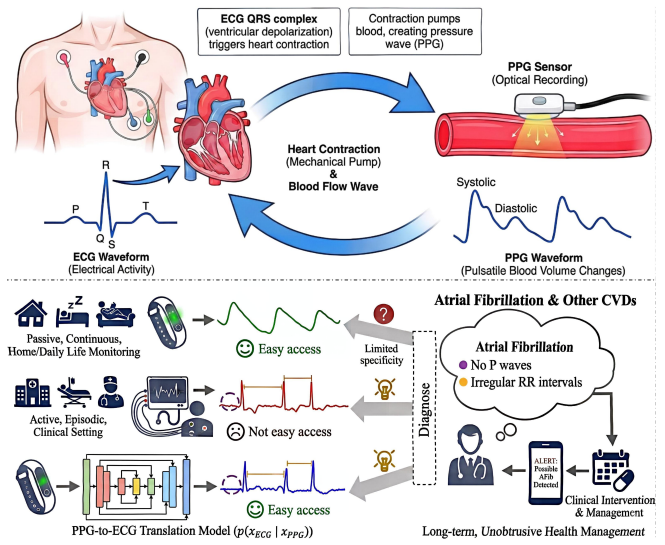


Figure 1: **Top:** Ventricular electrical activation on the ECG precedes and electromechanically initiates cardiac contraction, resulting in a delayed peripheral blood-volume pulse reflected in the PPG waveform. **Bottom:** PPG is easy to acquire but lacks diagnostic fidelity, whereas ECG reveals definitive disease markers. AI-based PPG-to-ECG translation offers a promising diagnostic pathway.

cess [Xie *et al.*, 2024; Li *et al.*, 2025]. However, short recording durations and the requirement for active user engagement still limit their suitability for long-term, passive monitoring and continuous health management [Nelson *et al.*, 2020].

Photoplethysmography (PPG) enables scalable, non-invasive, continuous monitoring and can be acquired in real time using widely deployed optical sensors. However, PPG does not directly capture cardiac electrophysiology, it provides limited diagnostic specificity for many CVDs. This creates a gap between accessible monitoring and diagnostic-grade assessment. As shown in Figure 1, PPG-to-ECG translation addresses this gap by inferring ECG-like waveforms or representations from PPG, enabling ECG-informed assessment when conventional ECG acquisition is unavailable. This is particularly relevant for long-term home monitoring, where standard ECG devices are less practical and sustained adherence is difficult. Compared with clinic-based ECG workflows that require visits and active participation, PPG-to-ECG

\*Equal contribution.

†Corresponding authors.

translation supports unobtrusive, longitudinal monitoring for high-risk individuals, facilitating chronic disease management, and earlier CVD screening.

Large-scale public datasets such as MCMED [Kansal *et al.*, 2025], which provide synchronized PPG–ECG recordings with curated CVD annotations, enable systematic development and evaluation of PPG-to-ECG translation methods for CVD diagnosis. Recent work has investigated diffusion models [Shome *et al.*, 2024] and flow-based models [Nambu *et al.*, 2025] for this task. While diffusion models often achieve strong synthesis quality, they typically require many iterative denoising steps, resulting in high inference latency. In contrast, flow-based models reduce inference cost by learning an explicit transformation from a simple noise distribution to the target signal, enabling sampling in a few steps.

Despite recent progress, PPG-to-ECG translation faces two major challenges: 1) **Physiological Semantics Misalignment in Generative Models**: Conventional end-to-end approaches often act as mere “waveform mimickers,” focusing on low-level signal reconstruction rather than physiological semantics. As a result, generated ECGs may resemble authentic waveforms morphologically but fail to preserve clinically actionable features essential for reliable cardiovascular disease screening and diagnosis, thereby limiting practical utility. 2) **Modeling Complexity in High-Dimensional Signals**: Complex temporal dependencies, inter-subject variability, and abrupt waveform transitions create highly non-smooth, modality-specific signal manifolds in raw data space. These properties violate the continuity and invertibility assumptions underlying conventional generative models, particularly flow-based architectures, leading to unstable training and poor generalization.

To address these challenges, we propose PPGFlowECG, a two-stage framework that couples CardioAlign Encoder with latent rectified flow for PPG-to-ECG translation and CVD detection. Stage 1 pretrains a cross-modal encoder-decoder with a shared CardioAlign encoder whose parameters are tied across PPG and ECG, encouraging modality-invariant cardiovascular representations beyond waveform-level similarity. Stage 2 trains a rectified-flow model in the latent space to learn a deterministic mapping from Gaussian noise to ECG latents via straight-line transport. Together, these stages yield ECGs with higher morphological fidelity and improved semantic consistency, facilitating clinical interpretation and downstream diagnosis. The main contributions are summarized as follows:

- We propose PPGFlowECG, a novel two-stage framework for high-fidelity PPG-to-ECG translation and cardiovascular disease detection. To our knowledge, this is *the first latent rectified flow model* specifically designed for cross-modal physiological signal generation.
- The proposed CardioAlign Encoder, together with multi-granularity latent constraints, induces a semantically aligned PPG–ECG latent space that couples naturally with latent rectified flow.
- We further provide a formal coupling analysis showing that latent alignment reduces conditional dispersion and vector-field curvature, improving numerical stability and

enabling efficient few-step sampling.

- We perform *the first large-scale evaluation on MCMED*, showing consistent gains in both translation quality and downstream disease detection. Cardiologist-led studies further suggests that our method can support real-world cardiovascular screening.

## 2 Related Work

Recent advances have spurred interest in generating ECG from PPG using generative models. Early studies relied on feature-engineered or transform-based pipelines to infer ECG characteristics from PPG waveforms [Banerjee *et al.*, 2014; Tian *et al.*, 2022; Zhu *et al.*, 2021]; for example, [Zhu *et al.*, 2021] used the Discrete Cosine Transform (DCT) to approximate cross-modal mappings. However, handcrafted approaches often fail to capture nonlinear physiological dependencies and can exhibit bias when applied to heterogeneous raw signals. More recent work therefore favors end-to-end deep generative modeling. CardioGAN [Sarkar and Etemad, 2021] adopts a CycleGAN-style framework for PPG-to-ECG translation under paired and unpaired supervision, and P2E-WGAN [Vo *et al.*, 2021] uses a conditional GAN with a Wasserstein objective to improve training stability and reconstruction quality. ADSSM [Vo *et al.*, 2024] formulates translation via variational inference with a Gaussian prior, whereas RDDM [Shome *et al.*, 2024] leverages diffusion to model region-wise waveform structure and improve morphological realism. CardioFlow [Nambu *et al.*, 2025] casts PPG-to-ECG translation as rectified flow, enabling one/few-step conditional generation by learning a velocity field from noise to ECG, and improves morphology via probabilistic peak masking that emphasizes QRS complexes and systolic peaks. Beyond translation, specialized architectures target downstream CVD detection; for instance, Performer [Lan, 2023] reconstructs ECGs with transformer-based models and combines them with native PPG to improve diagnostic performance. Despite the efficiency of rectified-flow translation (e.g., CardioFlow), learning flow dynamics directly in the raw waveform space can be unstable when cross-modal physiological semantics are not explicitly aligned. We therefore propose PPGFlowECG, which couples a shared semantically aligned latent space with latent rectified flow, and provide a formal analysis of this coupling.

## 3 Methodology

### 3.1 Overview of PPGFlowECG

PPGFlowECG generates ECGs from PPG in two stages: (i) a shared CardioAlign Encoder constructs a semantically aligned PPG–ECG latent space, and (ii) a PPG-conditioned latent rectified flow deterministically maps Gaussian noise to an ECG latent via straight-line transport, which is then decoded into a waveform. As illustrated in Figure 2, operating in the aligned latent space mitigates instability caused by non-smooth, modality-specific structure in the raw signal domain while preserving morphological fidelity and clinical interpretability in the synthesized ECGs.

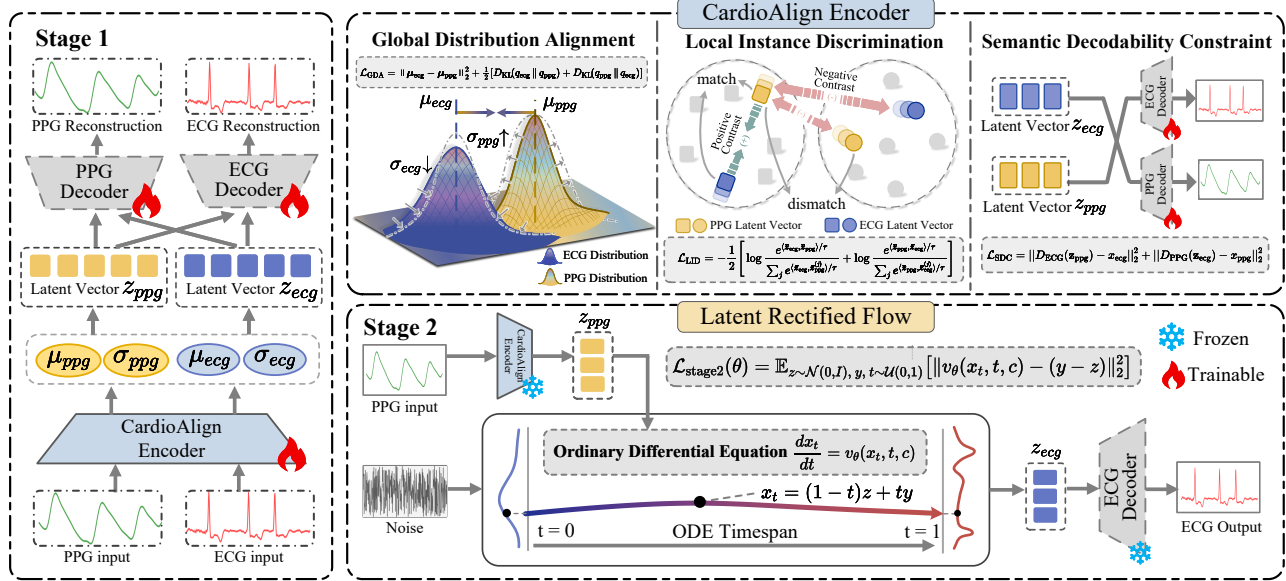


Figure 2: Illustration of the proposed PPGFlowECG framework for high-fidelity PPG-to-ECG translation and cardiovascular disease detection. In this figure, the framework aligns PPG and ECG in a shared latent space using the CardioAlign Encoder and employs latent rectified flow to synthesize ECGs with high fidelity and interpretability.

### 3.2 CardioAlign Encoder

PPG and ECG differ in surface morphology yet reflect the same underlying cardiovascular dynamics. When trained separately, modality-specific encoders may overfit modality-specific cues and miss shared physiological semantics. The CardioAlign Encoder mitigates this by using a shared encoder  $E_{CA}(\cdot)$  for both modalities, aligning them in a unified latent space and reducing sensitivity to waveform-specific appearance while retaining clinically relevant features for downstream diagnosis. Given an input waveform  $x_m \in \mathbb{R}^{L \times 1}$  from modality  $m \in \{\text{ppg}, \text{ecg}\}$ , the encoder outputs  $\mu_m$  and  $\sigma_m$ , and samples  $\mathbf{z}_m$  via the reparameterization trick:

$$\mathbf{z}_m = \mu_m + \sigma_m \odot \epsilon, \quad \epsilon \sim \mathcal{N}(\mathbf{0}, \mathbf{I}). \quad (1)$$

To induce a semantically coherent latent space, we adopt a coarse-to-fine alignment strategy at three levels, as follows:

**Global Distribution Alignment.** We initiate alignment at the distributional level by modeling each modality’s latent posterior as a Gaussian. Specifically, the posteriors for PPG and ECG, denoted as  $q_{\text{ppg}}$  and  $q_{\text{ecg}}$ , are defined as:

$$q_m = \mathcal{N}(\mu_m, \text{diag}(\sigma_m^2)), \quad m \in \{\text{ppg}, \text{ecg}\}, \quad (2)$$

where  $\mu_m$  denotes the posterior mean and  $\sigma_m^2$  denotes the posterior variance for modality  $m$ . To align these distributions,  $\mathcal{L}_{\text{GDA}}$  is defined as follow:

$$\begin{aligned} \mathcal{L}_{\text{GDA}} = & \|\mu_{\text{ecg}} - \mu_{\text{ppg}}\|_2^2 \\ & + \frac{1}{2} [D_{\text{KL}}(q_{\text{ecg}} \parallel q_{\text{ppg}}) + D_{\text{KL}}(q_{\text{ppg}} \parallel q_{\text{ecg}})], \end{aligned} \quad (3)$$

where the first term encourages mean alignment, and the symmetric Kullback-Leibler (KL) divergence [Zhang *et al.*, 2023] matches the dispersion of the two posteriors. Together, these terms provide a coarse-grained yet stable distribution-level constraint that mitigates collapse and promotes a shared physiological latent space.

**Local Instance Discrimination.** While global distribution alignment provides a stable coarse constraint across modalities, it lacks the granularity needed to preserve patient-specific cardiac signatures and rhythm-level variations. We therefore propose a Local Instance Discrimination (LID) mechanism. Let  $\bar{\mathbf{z}}_{\text{ecg}}$  and  $\bar{\mathbf{z}}_{\text{ppg}}$  denote mean-pooled latent representations. Paired segments are treated as positives, whereas cross-subject in-batch pairings serve as negatives, encouraging  $E_{CA}(\cdot)$  to align the two modalities while retaining subject-specific information.  $\mathcal{L}_{\text{LID}}$  is defined as follow:

$$\mathcal{L}_{\text{LID}} = -\frac{1}{2} \left[ \log \frac{e^{\langle \bar{\mathbf{z}}_{\text{ecg}}, \bar{\mathbf{z}}_{\text{ppg}} \rangle / \tau}}{\sum_j e^{\langle \bar{\mathbf{z}}_{\text{ecg}}, \bar{\mathbf{z}}_{\text{ppg}}^{(j)} \rangle / \tau}} + \log \frac{e^{\langle \bar{\mathbf{z}}_{\text{ppg}}, \bar{\mathbf{z}}_{\text{ecg}} \rangle / \tau}}{\sum_j e^{\langle \bar{\mathbf{z}}_{\text{ppg}}, \bar{\mathbf{z}}_{\text{ecg}}^{(j)} \rangle / \tau}} \right]. \quad (4)$$

By increasing similarity for matched cross-modal pairs and decreasing similarity for mismatched subjects,  $\mathcal{L}_{\text{LID}}$  mitigates representation over-smoothing in the aligned latent space and promotes subject-discriminative embeddings.

**Semantic Decodability Constraint.** While the objectives above establish coarse-to-fine cross-modal alignment, a unified representation should not only reside in a shared latent space but also support consistent cross-modal decoding. To impose this stronger functional constraint, we require the latent representation from one modality to reconstruct the other. This cross-modal decodability encourages the latent space to encode translatable physiological factors necessary for modality fusion. We define  $\mathcal{L}_{\text{SDC}}$  as follows:

$$\mathcal{L}_{\text{SDC}} = \|D_{\text{ECG}}(\mathbf{z}_{\text{ppg}}) - x_{\text{ecg}}\|_2^2 + \|D_{\text{PPG}}(\mathbf{z}_{\text{ecg}}) - x_{\text{ppg}}\|_2^2. \quad (5)$$

By enforcing  $\mathbf{z}_{\text{ppg}}$  to decode into ECG and  $\mathbf{z}_{\text{ecg}}$  into PPG, the latent space is driven to capture physiologically meaningful factors that generalize across modalities, thereby reinforcing cross-modal translatability. Overall,  $\mathcal{L}_{\text{CA}}$  is formulated as:

$$\mathcal{L}_{\text{CA}} = \mathcal{L}_{\text{GDA}} + \mathcal{L}_{\text{LID}} + \mathcal{L}_{\text{SDC}}. \quad (6)$$

### 3.3 Latent Rectified Flow

To enable high-fidelity ECG generation from PPG, we develop a generative model based on latent rectified flow. This formulation reduces generation to learning a straight-line vector field in a structured latent space. Rather than modeling flow dynamics directly in the raw waveform domain [Nambu *et al.*, 2025], we operate in the shared latent space, which is lower-dimensional and smoother. This choice better satisfies the continuity assumptions underlying flow models, improving training stability and enabling efficient sampling.

**Conditional Generative Modeling.** Building on the aligned latent manifold, we employ latent rectified flow to synthesize high-fidelity ECG signals. Specifically, we learn a conditional vector field  $v_\theta$  that transports samples from an isotropic Gaussian prior  $z \sim \mathcal{N}(\mathbf{0}, \mathbf{I})$  to the target ECG latent representation  $y$ . For interpolation time  $t \in [0, 1]$ , we define the probability-flow dynamics as follows:

$$x_t = (1 - t)z + ty. \quad (7)$$

Here,  $t = 0$  and  $t = 1$  correspond to the noise prior and the target latent, respectively. Under linear interpolation, the optimal drift (instantaneous velocity) is constant, i.e.,  $v^*(x_t, t, c) = y - z$ . The CardioAlign Encoder concentrates the conditional distribution  $p(y | c)$ , which in turn reduces the curvature of the learned vector field  $v_\theta(x_t, t, c)$ . We optimize  $v_\theta$  using a mean-squared error objective:

$$\mathcal{L}(\theta) = \mathbb{E}_{z \sim \mathcal{N}(0, I), y, t \sim \mathcal{U}(0, 1)} [\|v_\theta(x_t, t, c) - (y - z)\|_2^2] \quad (8)$$

To estimate  $v_\theta$ , we use a Transformer backbone with hierarchical cross-modal conditioning. The ECG latent  $y$  is projected into a compact token sequence via a 1D convolutional embedder, preserving local temporal structure while supporting long-range modeling. The PPG latent  $c$  conditions generation through cross-attention in every Transformer block, with  $c$  as key-value and the evolving ECG tokens as queries. This layerwise conditioning promotes fine-grained temporal alignment and physiological consistency along the generative trajectory, enabling clinically interpretable ECG synthesis with few ODE-solver steps.

**Inference and Sampling.** During inference, we synthesize an ECG signal conditioned on the PPG latent  $c$ . We first sample an initial noise vector  $z \sim \mathcal{N}(\mathbf{0}, \mathbf{I})$  as the starting point of the generative trajectory. The mapping from  $z$  to the target ECG latent  $y$  is then defined by an ODE [Hartman, 2002] governed by the learned conditional vector field  $v_\theta$ :

$$\frac{dx_t}{dt} = v_\theta(x_t, t, c), \quad t \in [0, 1]. \quad (9)$$

Here,  $x_t$  denotes the latent state at time  $t$ . To approximate the continuous trajectory, we use an explicit Euler solver with a fixed number of steps  $T$ . Let  $\Delta t = \frac{1}{T}$  and  $t_k = k, \Delta t$ . The latent state is updated iteratively as follows:

$$x_{k+1} = x_k + \Delta t \cdot v_\theta(x_k, t_k, c), \quad k = 0, 1, \dots, T - 1. \quad (10)$$

Finally, the terminal state  $x_T$  is taken as the generated ECG latent representation. This latent is then decoded by the frozen ECG decoder to reconstruct the synthesized ECG.

### 3.4 Why Latent Rectified Flow Fits CardioAlign?

The effectiveness of PPGFlowECG arises from coupling the CardioAlign Encoder with straight-line dynamics in latent rectified flow. This coupling can be formalized by analyzing how latent alignment shapes the optimization landscape and improves the numerical stability of the flow model.

**Conditional Dispersion and Regression Floor.** Let  $c = z_{\text{ppg}}$  and  $y = z_{\text{ecg}}$  denote the conditioning and target latents in the shared space. Stage 1 optimizes the CardioAlign objective  $\mathcal{L}_{\text{CA}}$ , which reduces the conditional dispersion of the target manifold. We quantify this dispersion using the average conditional variance,

$$\bar{\kappa} = \mathbb{E}_c [\text{tr}(\text{Cov}(y | c))]. \quad (11)$$

In Stage 2, rectified flow learns a vector field  $v_\theta$  by minimizing the mean-squared error to the straight-line drift  $y - z$ . The irreducible (Bayes) risk for this regression is as follows:

$$\mathcal{R}_{\min} = \mathbb{E}_{z \sim \mathcal{N}(0, I), y, t \sim \mathcal{U}(0, 1)} [\text{tr}(\text{Cov}(y - z | x_t, t, c))]. \quad (12)$$

Because  $z$  is sampled independently of  $(c, y)$ , the law of total variance implies  $\text{Cov}(y - z | x_t, t, c) \preceq \text{Cov}(y | c)$ , and therefore  $\mathcal{R}_{\min} \leq \bar{\kappa}$ . Therefore, Stage 1 reduces the irreducible noise floor for subsequent flow learning, facilitating the recovery of fine-grained ECG morphology.

**Trajectory Linearization and Numerical Stability.** Beyond reducing regression error, the benefit of coupling CardioAlign Encoder with latent rectified flow also appears as reduced curvature of the learned vector field. CardioAlign Encoder aligns  $y$  and  $c$  in a shared latent neighborhood. As  $\bar{\kappa} \rightarrow 0$ , the optimal drift approaches a spatially invariant field, i.e.,  $\nabla_x v^* \rightarrow \mathbf{0}$ . We quantify curvature through the second derivative along the trajectory,

$$x_t^{(2)} = \frac{d}{dt} v_\theta(x_t, t, c). \quad (13)$$

For the explicit Euler solver used at inference, the local truncation error scales as  $R_k = O(\Delta t^2 \|x_t^{(2)}\|_2)$ . Because Stage 1 alignment makes the target  $y$  close to the conditioning latent  $c$  in the aligned space, the learned dynamics are approximately linear, yielding  $x_t^{(2)} \approx 0$ . This reduces numerical error and supports stable generation with few ODE steps (e.g.,  $T \in \{5, 10\}$ ). Overall, Stage 1 alignment and Stage 2 rectified-flow generation are coupled to improve both efficiency and synthesis fidelity.

## 4 Experiments

### 4.1 Datasets and Evaluation Metrics

We evaluate PPGFlowECG on four datasets covering diverse clinical scenarios: MCMED [Kansal *et al.*, 2025], MIMIC-AFib [Bashar *et al.*, 2019], VitalDB [Lee *et al.*, 2022], and BIDMC [Pimentel *et al.*, 2016]. Following prior work [Shome *et al.*, 2024], we use Lead II ECG as the reference channel across all datasets. Reconstruction fidelity is measured by mean absolute error (MAE) and root mean

Methods	Ref.	MCMED					MIMIC-AFib				
		MAE ↓	RMSE ↓	FD ↓	FID ↓	MAE <sub>HR</sub> ↓	MAE ↓	RMSE ↓	FD ↓	FID ↓	MAE <sub>HR</sub> ↓
DDPM ( $T = 50$ ) [Ho <i>et al.</i> , 2020]	NIPS’20	0.94	1.36	<b>13.02</b>	44.72	7.00	<b>0.73</b>	<b>1.22</b>	107.20	42.86	9.55
CardioGAN [Sarkar and Etemad, 2021]	AAAI’21	0.98	1.40	80.19	53.54	<u>2.72</u>	<b>0.73</b>	<b>1.22</b>	64.19	45.86	<u>3.42</u>
Rectified Flow ( $T = 10$ ) [Liu <i>et al.</i> , 2022]	ICLR’22	0.97	1.36	104.35	54.71	26.40	0.83	1.36	68.28	49.30	26.01
RDDM ( $T = 10$ ) [Shome <i>et al.</i> , 2024]	AAAI’24	0.99	1.41	56.19	<u>20.81</u>	7.45	0.82	1.37	77.77	<u>42.57</u>	15.35
CardioFlow ( $T = 10$ ) [Nambu <i>et al.</i> , 2025]	ICASSP’25	0.95	1.35	85.84	48.12	15.37	0.76	1.33	65.28	44.39	17.92
<b>PPGFlowECG (<math>T = 10</math>)</b>	Ours	<b>0.73</b>	<b>1.14</b>	<u>43.99</u>	<b>12.84</b>	<b>1.80</b>	<b>0.73</b>	<u>1.29</u>	<b>63.75</b>	<b>37.69</b>	<b>2.30</b>

Methods	Ref.	VitalDB					BIDMC				
		MAE ↓	RMSE ↓	FD ↓	FID ↓	MAE <sub>HR</sub> ↓	MAE ↓	RMSE ↓	FD ↓	FID ↓	MAE <sub>HR</sub> ↓
DDPM ( $T = 50$ ) [Ho <i>et al.</i> , 2020]	NIPS’20	0.83	<u>1.31</u>	<b>40.76</b>	32.03	11.57	0.79	1.24	135.88	<u>54.88</u>	5.82
CardioGAN [Sarkar and Etemad, 2021]	AAAI’21	<u>0.82</u>	1.32	88.97	<b>20.92</b>	<u>3.50</u>	0.82	1.31	79.64	63.35	<b>1.38</b>
Rectified Flow ( $T = 50$ ) [Liu <i>et al.</i> , 2022]	ICLR’22	0.90	1.37	90.59	64.23	36.36	0.82	1.33	<u>74.48</u>	55.54	9.14
RDDM ( $T = 10$ ) [Shome <i>et al.</i> , 2024]	AAAI’24	0.87	1.40	131.74	64.62	30.27	0.83	1.34	89.81	63.06	10.23
CardioFlow ( $T = 10$ ) [Nambu <i>et al.</i> , 2025]	ICASSP’25	0.85	1.34	87.62	56.45	28.87	<u>0.79</u>	1.31	76.13	58.32	7.37
<b>PPGFlowECG (<math>T = 10</math>)</b>	Ours	<b>0.59</b>	<b>1.10</b>	<u>54.87</u>	<u>27.09</u>	<b>3.23</b>	<b>0.71</b>	<b>1.15</b>	<b>46.72</b>	<b>54.22</b>	<u>2.35</u>

Table 1: Comparison with state-of-the-art approaches on four datasets, including MCMED, MIMIC-AFib, VitalDB, and BIDMC.

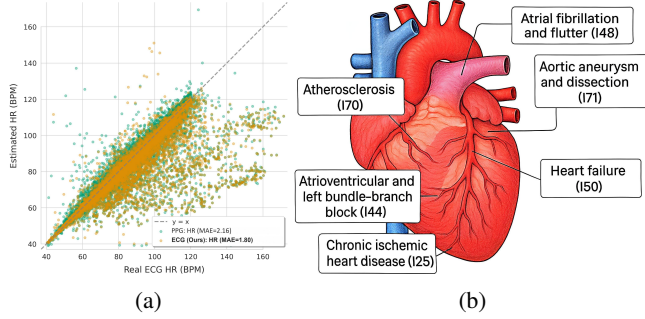


Figure 3: (a) A scatter plot comparing heart rate (HR) estimation accuracy and (b) An evaluation encompassing cardiovascular diseases across rhythm, conduction, vascular, and structural domains. square error (RMSE). To assess distributional similarity between real and synthesized signals, we report Fréchet Distance (FD) and Fréchet Inception Distance (FID), using ECG-Founder [Li *et al.*, 2024] as the feature extractor for FID. Heart rate (bpm) is estimated from real and synthesized ECGs with the Hamilton algorithm [Hamilton, 2002], and the heart-rate error is reported as MAE<sub>HR</sub>. For downstream evaluation, we report per-class AUROC and Macro-AUROC on MCMED, and accuracy and F1 score for binary atrial fibrillation classification on MIMIC-AFib.

## 4.2 Implementation Details and Baselines

ECG and PPG signals were preprocessed using standardized procedures to ensure data quality and cross-dataset consistency [Pan and Tompkins, 2007]. Continuous recordings were segmented into non-overlapping 10-s windows. All signals were resampled to 128 Hz and z-score normalized to mitigate differences in sampling rates and inter-subject variability. MCMED followed its official data split, whereas the remaining datasets were partitioned at the subject level into 80% training and 20% testing sets to prevent information leakage. We compare PPGFlowECG with representative GAN-, diffusion-, and flow-based generative baselines. All experiments were conducted on a single NVIDIA A800 GPU.

## 4.3 Comparisons with State-of-The-Arts

**Evaluation on PPG-to-ECG Translation.** Table 1 shows that the proposed method performs strongly across all evaluated metrics and datasets. PPGFlowECG achieves state-of-the-art or competitive results, indicating robust cross-dataset performance. We further evaluate whether PPG-to-ECG translation improves heart-rate (HR) estimation. As shown in Figure 3a, HR estimates derived from synthesized ECGs lie closer to the  $y = x$  identity line than those obtained directly from PPG. Consistent with this observation, synthesized ECGs yield a lower HR estimation MAE (1.80 vs. 2.16), corresponding to a 16.7% relative reduction.

**Evaluation on Cardiovascular Disease Detection.** We evaluate the clinical utility of synthesized ECGs via downstream diagnostic tasks on MCMED and MIMIC-AFib. For MCMED multi-label cardiovascular classification, as shown in Figure 3b, the selected ICD categories span diverse pathophysiological mechanisms, including rhythm, conduction, vascular, and structural disorders. For fair comparison, all methods are evaluated with the same Net-1d classifier [Hong *et al.*, 2020]. As reported in Table 2, PPGFlowECG achieves the best overall Macro-AUROC (0.631), improving over the strongest PPG-based baseline by 19.1% and over the best Gen.ECG-based baseline by 3.8%. For atrial fibrillation detection on MIMIC-AFib, evaluated as binary classification using a VGG-13 classifier [Sallem *et al.*, 2020], Table 3 shows that PPGFlowECG achieves 0.82 accuracy and 0.87 F1, corresponding to relative gains of 18.8%/16.0% over the best PPG-based method and 15.5%/4.8% over the best Gen.ECG-based method. Overall, these results suggest that ECGs synthesized by PPGFlowECG preserve diagnostically relevant information for downstream prediction.

## 4.4 Ablation Study

In the ablation study, we evaluate two degraded variants of PPGFlowECG to estimate the contribution of each stage. The Stage 1-only variant retains the CardioAlign Encoder and cross-modal decoders and is trained with cross-modal

Methods	Ref.	Disease Categories (AUROC) $\uparrow$						Macro-AUROC $\uparrow$
		I48	I71	I70	I44	I25	I50	
<b>PPG-based</b>								
PaPaGei [Pillai <i>et al.</i> , 2025]	ICLR’25	0.610	0.573	0.551	0.589	0.557	0.554	0.572
<b>Gen. ECG-based</b>								
DDPM ( $T = 50$ ) [Ho <i>et al.</i> , 2020]	NIPS’20	0.666	0.605	0.576	<b>0.625</b>	0.584	0.591	0.608
CardioGAN [Sarkar and Etemad, 2021]	AAAI’21	0.612	<b>0.657</b>	0.567	0.570	0.574	0.539	0.587
Rectified Flow ( $T = 10$ ) [Liu <i>et al.</i> , 2022]	ICLR’22	0.499	0.502	0.504	0.496	0.497	0.497	0.499
RDDM ( $T = 10$ ) [Shome <i>et al.</i> , 2024]	AAAI’24	0.574	0.576	0.538	0.573	0.544	0.525	0.555
CardioFlow ( $T = 10$ ) [Nambu <i>et al.</i> , 2025]	ICASSP’25	0.553	0.534	0.521	0.546	0.526	0.518	0.533
<b>PPGFlowECG (<math>T = 10</math>)</b>	Ours	<b>0.708</b>	0.626	<b>0.622</b>	0.619	<b>0.608</b>	<b>0.604</b>	<b>0.631</b>

Table 2: Quantitative evaluation of multi-label cardiovascular disease classification on the MCMED dataset.

Methods		Acc.	$\uparrow$	F1 $\uparrow$
<b>PPG-based</b>				
Shen et al. [Shen <i>et al.</i> , 2019]	SIGKDD’19	0.54	0.51	
PaPaGei [Pillai <i>et al.</i> , 2025]	ICLR’25	0.69	0.75	
<b>Gen. ECG-based</b>				
DDPM ( $T = 50$ ) [Ho <i>et al.</i> , 2020]	NIPS’20	0.70	0.80	
CardioGAN [Sarkar and Etemad, 2021]	AAAI’21	0.71	0.83	
Rectified Flow ( $T = 10$ ) [Liu <i>et al.</i> , 2022]	ICLR’22	0.61	0.71	
RDDM ( $T = 10$ ) [Shome <i>et al.</i> , 2024]	AAAI’24	0.70	0.82	
CardioFlow ( $T = 10$ ) [Nambu <i>et al.</i> , 2025]	ICASSP’25	0.68	0.77	
<b>PPGFlowECG (<math>T = 10</math>)</b>	Ours(Int.)	<b>0.82</b>	<b>0.87</b>	
<b>PPGFlowECG (<math>T = 10</math>)</b>	Ours(Ext.)	0.77	0.82	

Table 3: Classification performance for atrial fibrillation (AF) detection on the MIMIC-AFib dataset.

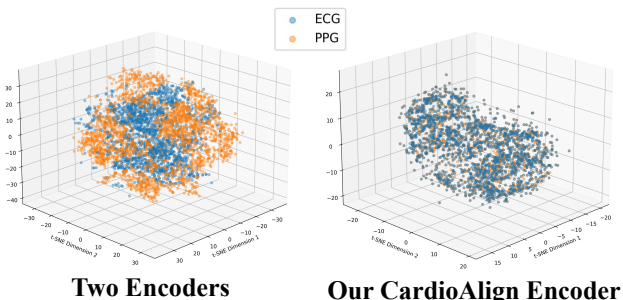


Figure 4: 3D t-SNE visualizations.

reconstruction, enabling direct PPG-to-ECG synthesis. The Stage 2-only variant adopts separate PPG and ECG encoders within a standard conditional rectified-flow pipeline, where the ECG encoder specifies the target latent and the PPG encoder provides conditioning. As shown in Table 4, the Stage 2-only variant performs worst, indicating that rectified-flow synthesis alone is insufficient without a Stage 1-aligned latent space. The Stage 1-only variant improves both metrics, supporting the role of a shared, semantically aligned manifold; however, without Stage 2 synthesis in this space, performance remains below the full model. Overall, the full model performs best, consistent with stage complementarity: Stage 1 aligns the latent space, and Stage 2 conducts straight-line transport within it to improve fidelity and preserve disease-discriminative content. We visualize modal-

Methods	MAE <sub>HR</sub> $\downarrow$	Macro-AUROC $\uparrow$
Only Stage 1	1.93	0.615
Only Stage 2	2.12	0.589
<b>PPGFlowECG</b>	<b>1.80</b>	<b>0.631</b>

Table 4: Ablation studies on the MCMED dataset.

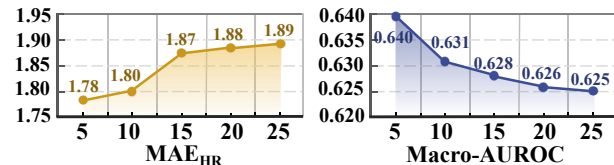


Figure 5: Ablation study of the effect of sampling steps.

ity separation by applying t-SNE [Maaten and Hinton, 2008] to project high-dimensional ECG and PPG representations into 3D, comparing CardioAlign Encoder with a baseline using two unaligned modality-specific encoders. In Fig. 4, the baseline shows distinct ECG and PPG clusters, indicating a pronounced modality gap. In contrast, our CardioAlign Encoder yields overlapping distributions, consistent with a more shared, modality-invariant latent space. This visualization indicates that the CardioAlign Encoder reduces the modality gap, which is associated with improved cross-modal generation fidelity. More evaluations and analysis are included in the *supplementary materials*.

#### 4.5 Parameter Analysis

To examine the effect of the ODE solver step count, we vary  $T$  from 5 to 25. As shown in Fig. 5, PPGFlowECG achieves its best performance at  $T = 5$ , and performance degrades as  $T$  increases. For the main experiments, we set  $T = 10$  to match the default inference setting of baseline methods (e.g., RDDM) and ensure comparable evaluation conditions. With  $T = 10$ , PPGFlowECG remains competitive across metrics.

#### 4.6 Generalization Analysis

To evaluate the zero-shot synthesis capability of our framework, we compare two settings: (i) internal validation, where the model is trained and tested on MIMIC-AFib, and (ii) external validation, where the model is trained on MCMED and directly evaluated on MIMIC-AFib without fine-tuning. As

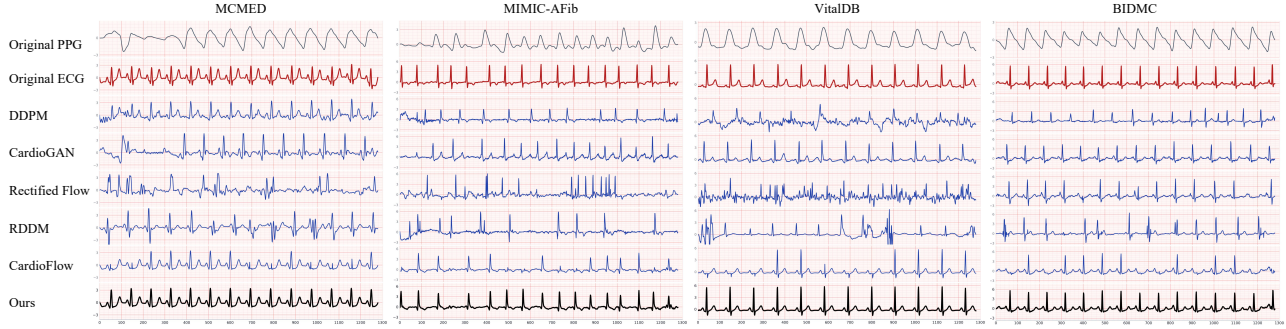


Figure 6: Comparison of synthesized ECGs generated by different models on multiple datasets.

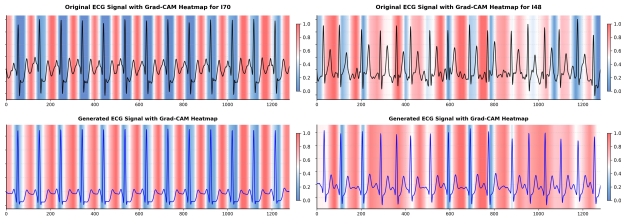


Figure 7: Explainability analysis with Grad-CAM on real (top) and synthesized (bottom) ECGs for two representative disease classes: I70 (left) and I48 (right).

shown in Table 3, the internal setting achieves 0.82 accuracy and 0.87 F1, whereas the external setting attains 0.77 accuracy and 0.82 F1. These results indicate strong zero-shot transfer with a modest performance drop, supporting practical deployment when paired target-domain data are limited.

## 4.7 Visualization Results

**Comparison of Synthesized ECGs.** We qualitatively compare synthesized waveforms across methods to assess ECG generation quality. As shown in Fig. 6, PPGFlowECG better preserves clinically relevant morphology, including sharper and better-aligned QRS complexes, more plausible ST-T dynamics, and fewer spurious oscillations. Overall, these examples suggest improved temporal coherence and closer agreement with real ECG waveform characteristics.

**Explainability Analysis with Grad-CAM.** We use Grad-CAM [Selvaraju *et al.*, 2017] to qualitatively assess whether synthesized ECGs induce classifier attributions on diagnostically relevant waveform regions. Using the same classifier, we compare attribution maps for real ECGs and PPGFlowECG-generated ECGs. As shown in Fig. 7, the maps exhibit partial correspondence between real and synthesized signals, with remaining discrepancies. Overall, these visualizations suggest that synthesized ECGs preserve task-relevant features leveraged by the downstream classifier.

## 4.8 Clinical Evaluation and Expert Assessment

**Clinical Turing Test.** In the first task, five board-certified cardiologists (one junior, three mid-level, and one senior) independently distinguished synthesized from real ECGs using a randomized set of 100 signals (50 real and 50 synthesized). As shown in Table 5, most experts’ identification accuracies

Metric	ID 1	ID 2	ID 3	ID 4	ID 5
Acc.	0.37	0.65	0.46	0.48	0.42
95% CI	[0.24, 0.52]	[0.50, 0.77]	[0.32, 0.61]	[0.34, 0.63]	[0.28, 0.57]

Table 5: Performance of five cardiologists on the Turing Test.

Test Modality	Acc. $\uparrow$	Sens. $\uparrow$	Spec. $\uparrow$
PPG only	$0.81 \pm 0.13$	$0.68 \pm 0.15$	$0.85 \pm 0.07$
PPG + Real ECG	$0.89 \pm 0.07$	$0.88 \pm 0.09$	$0.93 \pm 0.05$
PPG + Gen. ECG (Ours)	$0.87 \pm 0.09$	$0.92 \pm 0.04$	$0.88 \pm 0.11$

Table 6: Diagnostic performance of cardiologists for AF detection under different test modalities.

were near the chance level (0.50), with 95% confidence intervals overlapping 0.50. Although Expert 2 achieved a higher accuracy (0.65), the substantial inter-observer variability and consistently low detection rates indicate that the generated samples exhibit realistic morphological characteristics and are difficult to distinguish from clinical ground truth.

**Diagnostic Utility of Synthesized ECGs.** In the second task, five cardiologists diagnosed atrial fibrillation (AF) using 100 randomized signals (50 AF, 50 non-AF) under three conditions: PPG only, PPG+real ECG, and PPG+synthesized ECG. As shown in Table 6, the PPG-only condition yielded the lowest accuracy, sensitivity, and specificity. Adding real ECG achieved the highest accuracy ( $0.89 \pm 0.07$ ), with sensitivity and specificity of  $0.88 \pm 0.09$  and  $0.93 \pm 0.05$ . Using synthesized ECG resulted in comparable accuracy ( $0.87 \pm 0.09$ ) with higher sensitivity ( $0.92 \pm 0.04$ ) and lower specificity ( $0.88 \pm 0.11$ ) relative to real ECG. Overall, synthesized ECG provides clinically useful auxiliary information for AF detection and approaches the benefit of real ECG.

## 5 Conclusion

In this paper, we propose PPGFlowECG, a two-stage framework that aligns PPG and ECG in a shared latent space via the CardioAlign Encoder and synthesizes ECGs using latent rectified flow. By mitigating cross-modal semantic misalignment and the challenges of modeling high-dimensional waveform dynamics, PPGFlowECG achieves state-of-the-art performance in both reconstruction quality and downstream diagnostic tasks across multiple clinical settings. These results

support wearable-first cardiovascular screening and early detection when standard ECG acquisition is unavailable and only PPG is accessible.

## Statement on the Use of LLM

During this research and manuscript preparation, we used large language models (LLMs) exclusively for non-substantive assistance (e.g., drafting short utility scripts and supporting translation and language polishing). The study's hypotheses, methodology, experimental design, analyses, and conclusions are entirely the authors' independent work. LLMs were not used to generate or alter experimental data, to make methodological decisions, or to derive scientific conclusions. In addition, the top panel of Fig. 1 and Fig. 3b were generated with LLM assistance for visualization purposes; their scientific correctness and consistency with the described methods were thoroughly reviewed and verified by the authors. All LLM-assisted text/code/figures were critically reviewed and validated by the authors, who take full responsibility for the final content.

## References

[Banerjee *et al.*, 2014] Rohan Banerjee, Aniruddha Sinha, Anirban Dutta Choudhury, and Aishwarya Visvanathan. Photoecg: Photoplethysmography to estimate ecg parameters. In *IEEE International Conference on Acoustics, Speech and Signal Processing (ICASSP)*, pages 4404–4408. IEEE, 2014.

[Bashar *et al.*, 2019] Syed Khairul Bashar, Eric Ding, Alan J Walkey, David D McManus, and Ki H Chon. Noise detection in electrocardiogram signals for intensive care unit patients. *IEEE Access*, 7:88357–88368, 2019.

[Bayoumy *et al.*, 2021] Karim Bayoumy, Mohammed Gaber, Abdallah Elshafeey, Omar Mhaimeed, Elizabeth H Dineen, Francoise A Marvel, Seth S Martin, Evan D Muse, Mintu P Turakhia, Khaldoun G Tarakji, et al. Smart wearable devices in cardiovascular care: where we are and how to move forward. *Nature Reviews Cardiology*, 18(8):581–599, 2021.

[Chong *et al.*, 2024] Bryan Chong, Jayanth Jayabaskaran, Silingga Metta Jauhari, Siew Pang Chan, Rachel Goh, Martin Tze Wah Kueh, Henry Li, Yip Han Chin, Gwyneth Kong, Vickram Vijay Anand, et al. Global burden of cardiovascular diseases: projections from 2025 to 2050. *European Journal of Preventive Cardiology*, page zwaec281, 2024.

[Hamilton, 2002] Pat Hamilton. Open source ecg analysis. In *Computers in Cardiology*, pages 101–104. IEEE, 2002.

[Hartman, 2002] Philip Hartman. *Ordinary differential equations*. SIAM, 2002.

[Ho *et al.*, 2020] Jonathan Ho, Ajay Jain, and Pieter Abbeel. Denoising diffusion probabilistic models. *Advances in Neural Information Processing Systems (NeurIPS)*, 33:6840–6851, 2020.

[Hong *et al.*, 2020] Shenda Hong, Yanbo Xu, Alind Khare, Satria Priambada, Kevin Maher, Alaa Aljifry, Jimeng Sun, and Alexey Tumanov. Holmes: Health online model ensemble serving for deep learning models in intensive care units. In *Proceedings of the 26th ACM SIGKDD International Conference on Knowledge Discovery & Data Mining (KDD)*, pages 1614–1624, 2020.

[Kansal *et al.*, 2025] Aman Kansal, Emma Chen, Boyang Tom Jin, Pranav Rajpurkar, and David A Kim. Mc-med, multimodal clinical monitoring in the emergency department. *Scientific Data*, 12(1):1094, 2025.

[Kligfield *et al.*, 2007] Paul Kligfield, Leonard S Gettes, James J Bailey, Rory Childers, Barbara J Deal, E William Hancock, Gerard Van Herpen, Jan A Kors, Peter Macfarlane, David M Mirvis, et al. Recommendations for the standardization and interpretation of the electrocardiogram: part i: the electrocardiogram and its technology a scientific statement from the american heart association electrocardiography and arrhythmias committee, council on clinical cardiology; the american college of cardiology foundation; and the heart rhythm society endorsed by the international society for computerized electrocardiology. *Journal of the American College of Cardiology*, 49(10):1109–1127, 2007.

[Lan, 2023] Ella Lan. Performer: A novel ppg-to-ecg reconstruction transformer for a digital biomarker of cardiovascular disease detection. In *Proceedings of the IEEE/CVF Winter Conference on Applications of Computer Vision (WACV)*, pages 1991–1999, 2023.

[Lee *et al.*, 2022] Hyung-Chul Lee, Yoonsang Park, Soo Bin Yoon, Seong Mi Yang, Dongnyeok Park, and Chul-Woo Jung. Vitaldb, a high-fidelity multi-parameter vital signs database in surgical patients. *Scientific Data*, 9(1):279, 2022.

[Li *et al.*, 2024] Jun Li, Aaron Aguirre, Junior Moura, Che Liu, Lanhai Zhong, Chenxi Sun, Gari Clifford, Brandon Westover, and Shenda Hong. An electrocardiogram foundation model built on over 10 million recordings with external evaluation across multiple domains. *arXiv preprint arXiv:2410.04133*, 2024.

[Li *et al.*, 2025] Ding Li, Tian-Rui Cui, Jia-Hao Liu, Wan-Cheng Shao, Xiao Liu, Zhi-Kang Chen, Zi-Gan Xu, Xin Li, Shuo-Yan Xu, Zi-Yi Xie, et al. Motion-unrestricted dynamic electrocardiogram system utilizing imperceptible electronics. *Nature Communications*, 16(1):3259, 2025.

[Liu *et al.*, 2022] Xingchao Liu, Chengyue Gong, et al. Flow straight and fast: Learning to generate and transfer data with rectified flow. In *International Conference on Learning Representations (ICLR)*, 2022.

[Maaten and Hinton, 2008] Laurens van der Maaten and Geoffrey Hinton. Visualizing data using t-sne. *Journal of Machine Learning Research*, 9(Nov):2579–2605, 2008.

[Nambu *et al.*, 2025] Yuta Nambu, Masahiro Kohjima, and Ryuji Yamamoto. Cardioflow: Learning to generate ecg from ppg with rectified flow. In *ICASSP 2025-2025 IEEE International Conference on Acoustics, Speech and Signal Processing (ICASSP)*, pages 1–5. IEEE, 2025.

[Nelson *et al.*, 2020] Benjamin W Nelson, Carissa A Low, Nicholas Jacobson, Patricia Areán, John Torous, and Nicholas B Allen. Guidelines for wrist-worn consumer wearable assessment of heart rate in biobehavioral research. *NPJ Digital Medicine*, 3(1):90, 2020.

[Pan and Tompkins, 2007] Jiapu Pan and Willis J Tompkins. A real-time qrs detection algorithm. *IEEE Transactions on Biomedical Engineering*, (3):230–236, 2007.

[Pillai *et al.*, 2025] Arvind Pillai, Dimitris Spathis, Fahim Kawsar, and Mohammad Malekzadeh. Papagei: Open foundation models for optical physiological signals. In *The Thirteenth International Conference on Learning Representations*, 2025.

[Pimentel *et al.*, 2016] Marco AF Pimentel, Alistair EW Johnson, Peter H Charlton, Drew Birrenkott, Peter J Watkinson, Lionel Tarassenko, and David A Clifton. Toward a robust estimation of respiratory rate from pulse oximeters. *IEEE Transactions on Biomedical Engineering*, 64(8):1914–1923, 2016.

[Sallem *et al.*, 2020] Marwen Sallem, Amina Ghrissi, Adnen Saadaoui, and Vicente Zarzoso. Detection of cardiac arrhythmias from varied length multichannel electrocardiogram recordings using deep convolutional neural networks. In *2020 Computing in Cardiology*, pages 1–4. IEEE, 2020.

[Sarkar and Etemad, 2021] Pritam Sarkar and Ali Etemad. Cardiogan: Attentive generative adversarial network with dual discriminators for synthesis of ecg from ppg. In *Proceedings of the AAAI Conference on Artificial Intelligence (AAAI)*, volume 35, pages 488–496, 2021.

[Selvaraju *et al.*, 2017] Ramprasaath R Selvaraju, Michael Cogswell, Abhishek Das, Ramakrishna Vedantam, Devi Parikh, and Dhruv Batra. Grad-cam: Visual explanations from deep networks via gradient-based localization. In *Proceedings of the IEEE International Conference on Computer Vision (ICCV)*, pages 618–626, 2017.

[Shen *et al.*, 2019] Yichen Shen, Maxime Voisin, Alireza Aliamiri, Anand Avati, Awni Hannun, and Andrew Ng. Ambulatory atrial fibrillation monitoring using wearable photoplethysmography with deep learning. In *Proceedings of the 25th ACM SIGKDD international conference on knowledge discovery & data mining*, pages 1909–1916, 2019.

[Shome *et al.*, 2024] Debaditya Shome, Pritam Sarkar, and Ali Etemad. Region-disentangled diffusion model for high-fidelity ppg-to-ecg translation. In *Proceedings of the AAAI Conference on Artificial Intelligence (AAAI)*, volume 38, pages 15009–15019, 2024.

[Tian *et al.*, 2022] Xin Tian, Qiang Zhu, Yuenan Li, and Min Wu. Cross-domain joint dictionary learning for ecg inference from ppg. *IEEE Internet of Things Journal*, 10(9):8140–8154, 2022.

[Timmis *et al.*, 2022] Adam Timmis, Panos Vardas, Nick Townsend, Aleksandra Torbica, Hugo Katus, Delphine De Smedt, Chris P Gale, Aldo P Maggioni, Steffen E Petersen, Radu Huculeci, et al. European society of cardiology: cardiovascular disease statistics 2021. *European Heart Journal*, 43(8):716–799, 2022.

[Vaduganathan *et al.*, 2022] Muthiah Vaduganathan, George A Mensah, Justine Varieur Turco, Valentin Fuster, and Gregory A Roth. The global burden of cardiovascular diseases and risk: a compass for future health, 2022.

[Vo *et al.*, 2021] Khuong Vo, Emad Kasaeyan Naeini, Amir Naderi, Daniel Jilani, Amir M Rahmani, Nikil Dutt, and Hung Cao. P2e-wgan: Ecg waveform synthesis from ppg with conditional wasserstein generative adversarial networks. In *Proceedings of the 36th Annual ACM Symposium on Applied Computing*, pages 1030–1036, 2021.

[Vo *et al.*, 2024] Khuong Vo, Mostafa El-Khamy, and Yoojin Choi. Ppg-to-ecg signal translation for continuous atrial fibrillation detection via attention-based deep state-space modeling. In *2024 46th Annual International Conference of the IEEE Engineering in Medicine and Biology Society (EMBC)*, pages 1–7. IEEE, 2024.

[Xie *et al.*, 2024] Yingxi Xie, Longsheng Lu, Wentao Wang, and Huan Ma. Wearable multilead ecg sensing systems using on-skin stretchable and breathable dry adhesives. *Bio-Design and Manufacturing*, 7(2):167–180, 2024.

[Zhang *et al.*, 2023] Yufeng Zhang, Jialu Pan, Li Ken Li, Wanwei Liu, Zhenbang Chen, Xinwang Liu, and Ji Wang. On the properties of kullback-leibler divergence between multivariate gaussian distributions. *Advances in Neural Information Processing Systems (NeurIPS)*, 36:58152–58165, 2023.

[Zhu *et al.*, 2021] Qiang Zhu, Xin Tian, Chau-Wai Wong, and Min Wu. Learning your heart actions from pulse: Ecg waveform reconstruction from ppg. *IEEE Internet of Things Journal*, 8(23):16734–16748, 2021.